Performance Limits of Monolayer Transition Metal Dichalcogenide Transistors

Leitao Liu, S. Bala Kumar, Yijian Ouyang, and Jing Guo

***Abstract*—The performance limits of monolayer transition metal dichalcogenide (MX_2) transistors are examined with a ballistic MOSFET model. Using an *ab initio* theory, we calculate the band structures of 2-D transition MX_2. We find the lattice structures of monolayer MX_2 remain the same as the bulk MX_2. Within the ballistic regime, the performances of monolayer MX_2 transistors are better compared with those of the silicon transistors if a thin high-κ gate insulator is used. This makes monolayer MX_2 promising 2-D materials for future nanoelectronic device applications.**

***Index Terms*—*Ab initio* theory, ballistic transport, band structure calculation, new direct-gap semiconductor, 2-D transition metal dichalcogenide (MX_2).**

I. Introduction

GRAPHENE, A 2-D material with great electrical, thermal, and mechanical properties, has been widely studied in the past several years [1], [2]. However, due to the absence of band gap, the graphene-based field-effect transistors (FETs) have high OFF-currents. Therefore, different approaches are proposed to induce a band gap in graphene, e.g., lateral confinement into nanoribbons. However, these approaches often result in a significant reduction of carrier mobility [3], [4], loss of coherence [5], and increased OFF-current [6] compared to graphene.

Metal dichalcogenide $(MX_2)(\mathrm{M} = \mathrm{Mo}$ and W; $\mathrm{X} = \mathrm{S}, \mathrm{Se}, \mathrm{and}\ \mathrm{Te})$ belongs to the family of layered transition metal dichalcogenide, whose crystal structure is built up of X–M–X monolayers interacted through van der Waals forces. Each monolayer consists of two X atom layers and an M atom layer sandwiched between the X atom layers. Previous research found that MX_2 has a band gap of 1.1–2 eV [7], [8]. Therefore, a monolayer of semiconducting MX_2, which is a 2-D material, may be suitable for CMOS-like logic device applications and may be a promising replacement for silicon (Si). A scotch-tape-based micromechanical cleavage technique can be used to extract a stable single-layer MX_2 [9], [10]. In addition, liquid exfoliation approaches have been also proposed to produce 2-D nanosheets [11], [12]. It has been successfully shown that layered materials such as MoS_2, $MoSe_2$, $MoTe_2$, WS_2, $TaSe_2$, $NbSe_2$, $NiTe_2$, BN, and Bi_2Te_3 can be efficiently exfoliated into individual layers [12]. The research on electronic devices based on these novel 2-D materials has been greatly advanced due to these exfoliation techniques. The first successful realization of a FET based on monolayer MoS_2 has been reported with both high carrier mobility and high ON/OFF current ratio [13].

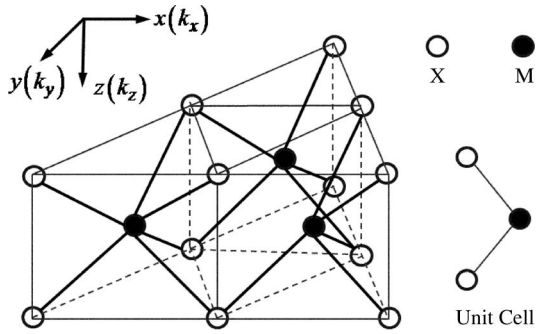

Fig. 1. Crystal structure of monolayer MX_2. The atoms form a trigonal prismatic coordination, and a hexagonal M atom layer is sandwiched between two hexagonal X atom layers. a is the lattice constant, and c is the height of the X–M–X layer.

Although monolayer MX_2-based transistors have been experimentally demonstrated, there is lack of theoretical investigations on their device performances. Thus, a comprehensive study and comparison of performance limits of these transistors from a theoretical model would be essential. In this paper, we first investigate the band structures of monolayer MX_2 using an *ab initio* theory and calculate their effective masses through fitting the band structures. Then, we examine the ballistic performance limits of a MOSFET with these materials as the channel materials and make a comparison with Si thin-film (2-D-Si) FETs.

II. Approach

A. Electronic Band Structure Calculation

Fig. 1 shows the atomic structure of $MX_2(\mathrm{M} = \mathrm{Mo}$ and W; $\mathrm{X} = \mathrm{S}, \mathrm{Se}, \mathrm{and}\ \mathrm{Te})$. MX_2 is a layered material that is composed of vertically stacked X–M–X layers through van der Waals forces. Each single X–M–X sandwich layer consists of two hexagonal planes of X atoms and an intermediate hexagonal plane of M atoms interacting through ionic–covalent interactions with a triangular prismatic coordination.

We employ the Vienna *ab initio* simulation package [14], [15] to perform density functional theory calculations, within the formalism of the projector augmented-wave method [16].

Manuscript received April 7, 2011; revised May 13, 2011; accepted June 1, 2011. Date of publication July 22, 2011; date of current version August 24, 2011. The review of this paper was arranged by Editor A. Schenk.

The authors are with the Department of Electrical and Computer Engineering, NEB 551, University of Florida, Gainesville, FL 32611 USA.

Digital Object Identifier 10.1109/TED.2011.2159221

0018-9383/$26.00 © 2011 IEEE

A double-zeta polarized basis set is used. The generalized gradient approximation (GGA) corrected functional by Perdew *et al.* [17] is used for the exchange-correlation potential. The cutoff energy for the wave-function expansion is set to 500 eV, and a mesh of $18 \times 18 \times 1$ k points is used for 2-D Brillouin-zone integrations.

We calculate the band structure of monolayer MoS_2 using three different methods. In the first method, we perform a regular GGA calculation, where we relax the structure first, and then calculate the band structure. The calculated band gap $E_g = 1.68$ eV. In the second method, we perform structure relaxation and band structure calculation using HSE06 [18] and obtain $E_g = 2.27$ eV. Compared with the reported experimental value of the band gap (1.8 eV) [19], above GGA and HSE06 calculations in the regular methods do not accurately predict the band gap of monolayer MoS_2. Therefore, in the third method, we construct the lattice structure of monolayer MoS_2 by using the measured bulk MoS_2 and perform band structure calculation without structure relaxation. The calculated band gap is 1.78 eV, which is in closer agreement with the experimental value compared with the previous two calculations. This indicates that the structure of monolayer MoS_2 is likely to remain the same as the bulk MoS_2 [10], [20]. Therefore, we adopt the third method for band structure calculations. However, note that, until present, there is no direct experimental evidence that indicates that the structure of a single-layer MoS_2 is indeed the same as the bulk one. Based on our calculations, the band structures of monolayer MX_2 are shown in Fig. 2. The band gap of monolayer MX_2 occurs at the high-symmetry *k* point, and it is direct, unlike the bulk MX_2 [19], [21]. We calculate the effective masses by a parabolic fitting of the band structure along corresponding crystal directions. The calculation results for MX_2 are listed in Table I.

B. Ballistic Performance Limits

Here, we use the analytical ballistic MOSFET model [25]–[29] to investigate the performance limits of transistors with monolayer MX_2 semiconductors as the channel materials. Fig. 3 illustrates the structure of the device used in the simulation, and Fig. 4(a) illustrates the potential barrier and the source and drain Fermi energy levels. At zero terminal bias, the equilibrium electron density at the top of energy barrier is

$$N_0 = \int_{-\infty}^{+\infty} D(E) f(E - E_F) dE \tag{1}$$

where $D(E)$ is the density of states at energy E, and $f(E - E_F)$ is the Fermi distribution with E_F as the Fermi level. When the gate and drain biases are applied, the energy barrier is accordingly modulated. The positive velocity states at the top of the barrier are filled by electrons from the source, and the negative states are filled by electrons from the drain. The electron density is given by

$$N = \frac{1}{2} \int_{-\infty}^{+\infty} D(E - U_{\mathrm{scf}}) [f(E - E_{\mathrm{FS}}) + f(E - E_{\mathrm{FD}})] \, dE \tag{2}$$

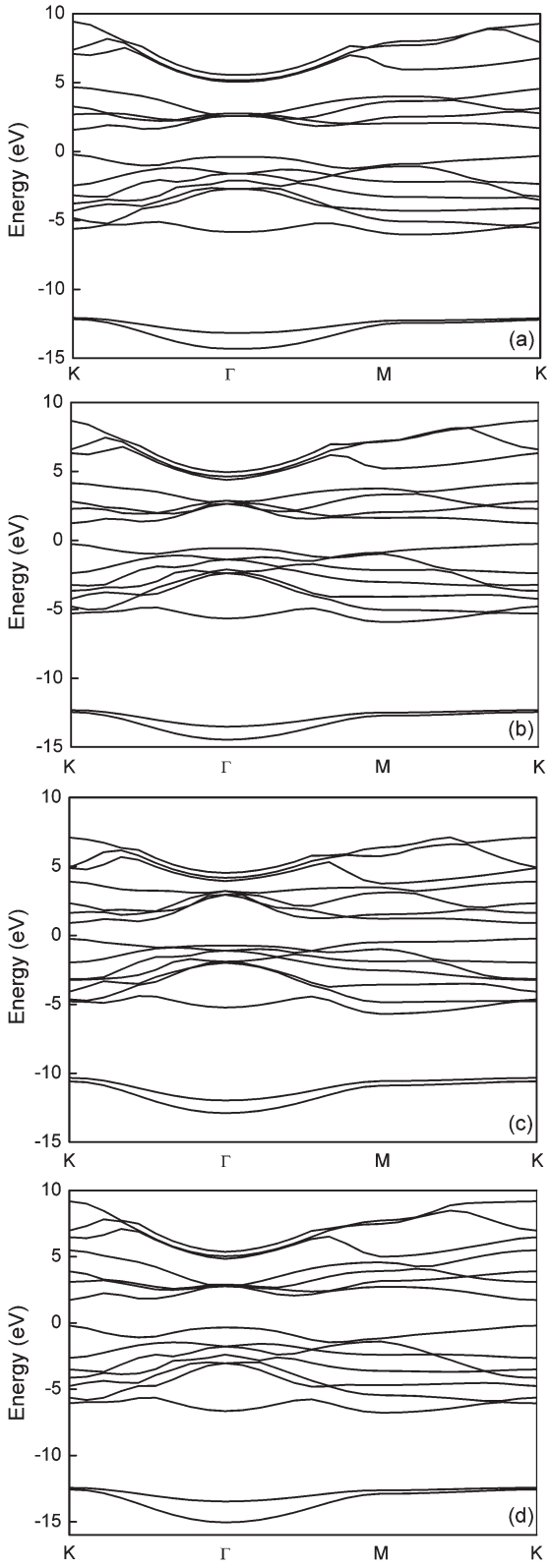

Fig. 2. Band structure of monolayer MX_2 calculated with a fixed crystal structure constructed by the bulk lattice parameters using GGA. The Fermi level is set at 0 eV. These materials are direct semiconductors, and the band gap occurs at the high-symmetry *k* point. (a) Monolayer MoS_2, $E_F = -3.5071$ eV. (b) Monolayer $MoSe_2$, $E_F = -3.1357$ eV. (c) Monolayer $MoTe_2$, $E_F = -2.3308$ eV. (d) Monolayer WS_2, $E_F = -3.2378$ eV.

TABLE I
CALCULATED RESULTS OF MONOLAYER MX_2 USING GGA

	MoS_2	$MoSe_2$	$MoTe_2$	WS_2
a (Å)	$3.16^{(1)}$	$3.299^{(1)}$	$3.522^{(1)}$	$3.1532^{(1)}$
	$3.182^{(2)}$	$3.311^{(2)}$	$3.539^{(2)}$	$3.181^{(2)}$
c (Å)	$3.172^{(1)}$	$3.338^{(1)}$	$3.604^{(1)}$	$3.1424^{(1)}$
	$3.138^{(2)}$	$3.348^{(2)}$	$3.622^{(2)}$	$3.140^{(2)}$
E_g (eV)	$1.78^{(3)}$	$1.49^{(3)}$	$1.13^{(3)}$	$1.93^{(3)}$
m_n^x ($\times m_0$)	$0.5788^{(3)}$	$0.6059^{(3)}$	$0.6164^{(3)}$	$0.3466^{(3)}$
m_n^y ($\times m_0$)	$0.5664^{(3)}$	$0.5933^{(3)}$	$0.6033^{(3)}$	$0.3382^{(3)}$
m_p^x ($\times m_0$)	$0.6659^{(3)}$	$0.7114^{(3)}$	$0.7586^{(3)}$	$0.4619^{(3)}$
m_p^y ($\times m_0$)	$0.6524^{(3)}$	$0.6967^{(3)}$	$0.7406^{(3)}$	$0.4501^{(3)}$

E_g is the energy band gap. $m_n^x\left(m_n^y\right)$ and $m_p^x\left(m_p^y\right)$ is the fitting effective mass for electron and hole along the $k_x\,(k_y)$ direction, respectively.
(1) Experimental data of bulk lattice parameters [7][8][22][23][24]
(2) Calculated data monolayer MX_2 lattice parameters by GGA with structure relaxation.
(3) Fitting parameters against band structure calculated by GGA with a fixed structure (using bulk lattice parameters in (1)).

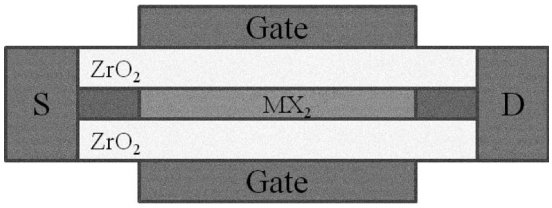

Fig. 3. Structure of a double-gate MOSFET model. The thickness of the ZrO_2 dielectric insulator $t_{\rm ins} = 3$ nm.

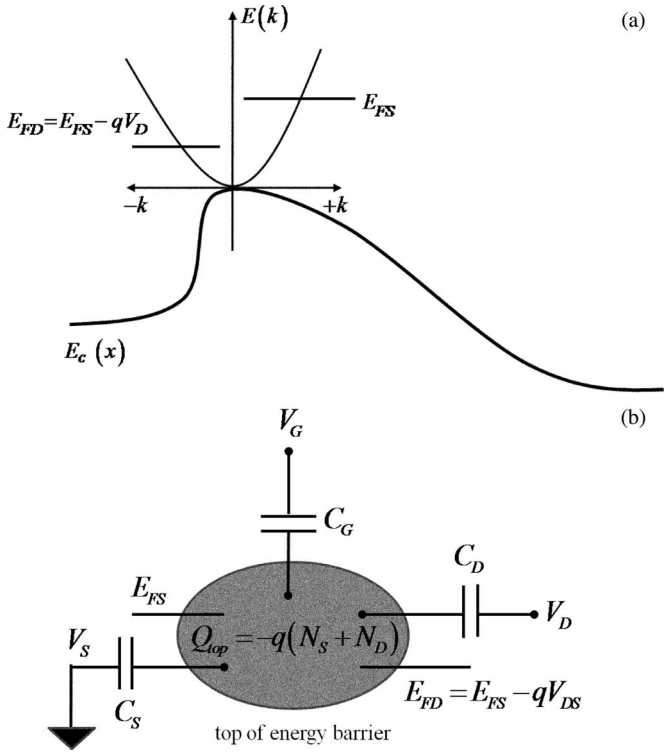

Fig. 4. (a) Illustration of the potential barrier and the source and drain Fermi energy levels. The $+k$ states are occupied by a carrier from the source, and the $-k$ states are occupied by a carrier from the drain. (b) Two-dimensional transistor model of ballistic MOSFET. The potential $U_{\rm scf}$ at the top of the energy barrier is controlled by the gate, source, and drain through the three capacitors, i.e., C_G, C_S, and C_D, respectively.

where $E_{\rm FS} and E_{\rm FD}$ are the Fermi levels in the source and the drain, respectively, and $U_{\rm scf}$ is the self-consistent surface potential, which is calculated by coupling the charge density calculation to a capacitance model that describes transistor electrostatics, as shown in Fig. 4(b), i.e.,

$$U_{\rm scf} = U_L + U_P \tag{3}$$

$$U_L = -q(\alpha_G V_G + \alpha_D V_D + \alpha_S V_S) \tag{4}$$

$$U_P = \frac{q^2}{C_G + C_D + C_S}(N - N_0) \tag{5}$$

where $\alpha_G = C_G/(C_G + C_D + C_S)$, $\alpha_D = C_D/(C_G + C_D + C_S)$, and $\alpha_S = C_S/(C_G + C_D + C_S)$. Once the convergence is achieved, ballistic current I_{DS} can be evaluated through the difference between the flux from the source and the drain. Then, the average electron velocity $v_{\rm avg}$ at the top of the barrier is then evaluated as

$$v_{\rm avg} = \frac{I_{DS}}{Q} = \frac{I_{DS}}{qN}. \tag{6}$$

Detailed derivations of this model are described in [27]. For comparison, we also include the simulated results of 2-D-Si transistors at the same operating bias. The thickness of a silicon thin film is set to 5 nm, and hence, three subbands are considered for n-type 2-D-Si transistors.

III. RESULTS AND DISCUSSIONS

As shown in Fig. 3, here we use a double-gate MOSFET with a high-κ $ZrO_2(\varepsilon_r = 25)$ dielectric insulator thickness $t_{\rm ins} = 3$ nm, which results in a gate capacitance value of $C_G = 0.1476$ pF/μm^2. However, for 2-D-Si transistors, since the quantum–mechanical effect in the direction that is normal to the interface between the channel and the gate insulator is significant, the average inversion layer actually locates away from the interface, increasing the total insulator layer thickness equivalently. The additional thickness of the insulator can be simply calculated as follows [30]:

$$\Delta t_{\rm ins} = \frac{\varepsilon_{\rm ins}}{\varepsilon_{\rm Si}} \times \Delta x_{\rm av} \tag{7}$$

where $\varepsilon_{\rm ins}$ is the relative permittivity of the gate dielectric, $\varepsilon_{\rm Si}$ is the relative permittivity of Si, and the difference of the depth of the inversion layer to the surface with and without a quantum–mechanical effect $\Delta x_{\rm av} = 10 - 12$ Å [30]. This value is valid for a wide range of channel doping and effective fields. In addition, a thin SiO_2 is formed at the surface of Si, even when a high-κ gate insulator material is used. In contrast, there are no dangling bonds and, therefore, no formation native oxide on the surface of monolayer MX_2. This effect results in a further increase in the total gate insulator thickness in 2-D-Si transistors. Therefore, the gate control on the channel charge density for monolayer MX_2 transistors is stronger than that

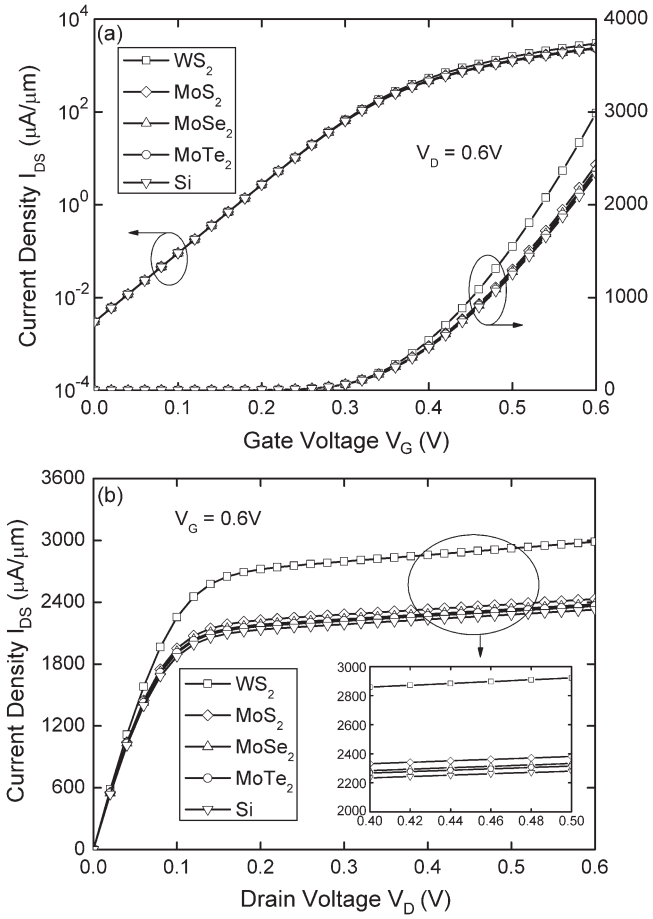

Fig. 5. Ballistic I–V characteristic comparison of n-type monolayer MX_2 and 2-D-Si transistors. Three subbands are considered in the calculation for a Si thin film. The OFF-current is set to be 0.003 μA/μm. (a) $I_{DS} \sim V_G$ with $V_D = 0.6$ V. (b) $I_{DS} \sim V_D$ with $V_G = 0.6$ V.

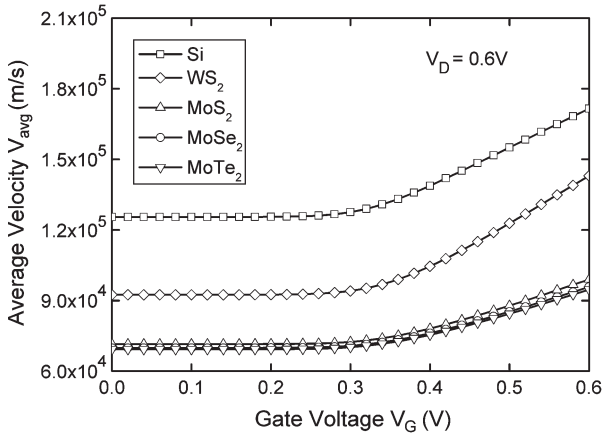

Fig. 6. Average velocity $V_{\rm avg}$ of carrier at the top of the energy barrier, with increasing gate voltage V_G for n-type monolayer MX_2 and 2-D-Si transistors. Three subbands are considered in the calculation for a Si thin film. V_D is set at 0.6 V.

for 2-D-Si transistors at any given biases. Due to the effects discussed above, here we use an equivalent ZrO_2 thickness of 5.5 nm for 2-D-Si transistors.

Before implementing the analytical model described above, we identify first the parameters, i.e., α_G, α_S, and α_D. These parameters represent the controllability of corresponding terminal on the modulation of the energy barrier. For an ideal MOSFET, the gate completely controls the potential, whereas the influence of the source and the drain are negligible, i.e., $\alpha_G \approx 1$ and α_S and $\alpha_D \approx 0$. In a more realistic case, these parameters can be obtained by fitting the experimental results. Here, we set $\alpha_G = 0.88$ and $\alpha_D = 0.035$, respectively. To compare the performances of transistors with different channel materials, we adjust $E_{\rm FS}$ to achieve a fixed OFF-current density of 0.003 μA/μm. $E_{\rm FS}$ can be adjusted by changing the work function of the gate and the doping density in the source. Note that the Fermi level used in our calculations (intrinsic Fermi level) of MoS_2, $MoSe_2$, $MoTe_2$, and WS_2 are -0.3406 (-3.5071), -0.3412 (-3.1357), -0.3414 (-2.3308), and -0.3340 (-3.2378) eV, respectively.

The calculated results of an n-type MOSFET along the k_x-direction are presented in Fig. 5. Fig. 5(a) and (b) shows the I_{DS}–V_G and I_{DS}–V_D characteristics, respectively. All the monolayer MoX_2 transistors, i.e., MoS_2, $MoSe_2$, and $MoTe_2$, have similar values for the ON-current, and these values are slightly higher than those of the 2-D-Si transistors. On the other hand, within the ballistic regime, the monolayer WS_2 transistors have the best performance. WS_2 transistors outperform 2-D-Si transistors in terms of ON-current by about 28.3%. Due to the atomic body thickness of monolayer MX_2, transistors with these materials exhibit good gate control and result in a high ON-current. This makes monolayer MX_2 to be promising channel materials to replace Si for future FETs. Fig. 6 shows the average velocity of electron versus the gate voltage at $V_D = 0.6$ V. The electron transport effective mass of monolayer MX_2 is larger than that of 2-D-Si, and hence, the electron velocity in monolayer MX_2 transistors is lower than that in 2-D-Si transistors. In addition, the performances of all the different monolayer MoX_2 transistors are similar due to the similarity in the electron effective masses.

The calculated results of a p-type MOSFET along the k_x-direction are presented in Figs. 7 and 8. Here, we consider both the heavy and light holes of Si. The p-type MOSFET shows similar conclusions as the n-type MOSFETs. The ON-current of monolayer WS_2 transistors is 1.5 times larger than that of 2-D-Si transistors. Moreover, monolayer MoS_2 transistors outperform 2-D-Si transistors in terms of ON-current by about 27.3%.

Note that we also evaluate ballistic performances along the other crystal direction, i.e., the k_y-direction, and find that the results are very close to those along the k_x-direction with a difference of less than 3%. Therefore, we have only presented the results for the k_x-direction.

Finally, we study the effect of using a thicker gate oxide on the transistor performance. For a thicker gate oxide, the decrease in the gate capacitance due to quantum effects and silicon native oxide is less important. For a SiO_2 gate insulator thickness of 10 nm, the 2-D-Si transistors deliver a 20.6% larger ON-current than the monolayer WS_2 transistors, because the larger carrier velocity has a more dominant effect than slight degradation of the gate capacitance in 2-D-Si MOSFETs, as previously discussed. Therefore, to exploit the performance

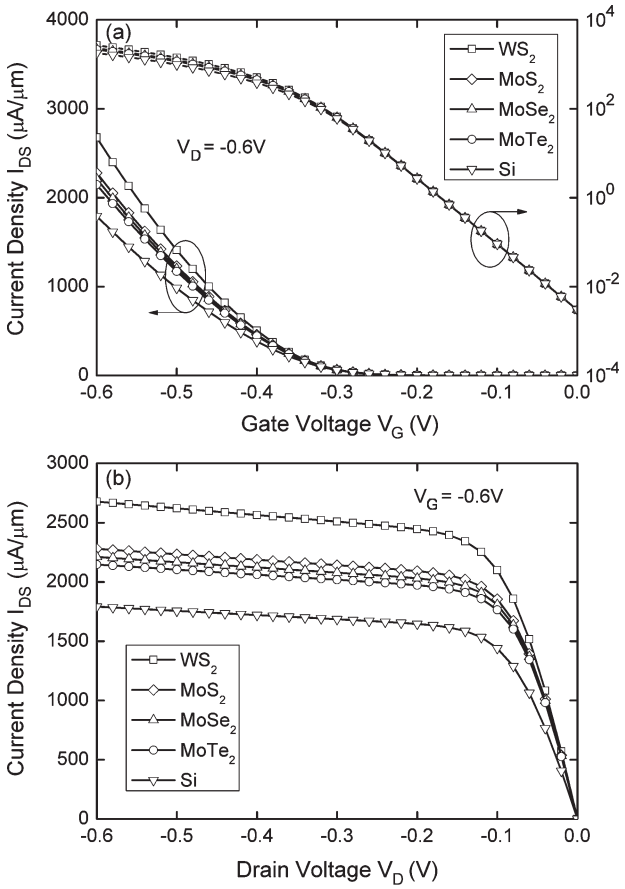

Fig. 7. Ballistic I–V characteristic comparison of p-type monolayer MX_2 and 2-D-Si transistors. Both the heavy and light holes of Si are considered in the calculation. The OFF-current is set to be 0.003 μA/μm. (a) $I_{DS} \sim V_G$ with $V_D = -0.6$ V. (b) $I_{DS} \sim V_D$ with $V_G = -0.6$ V.

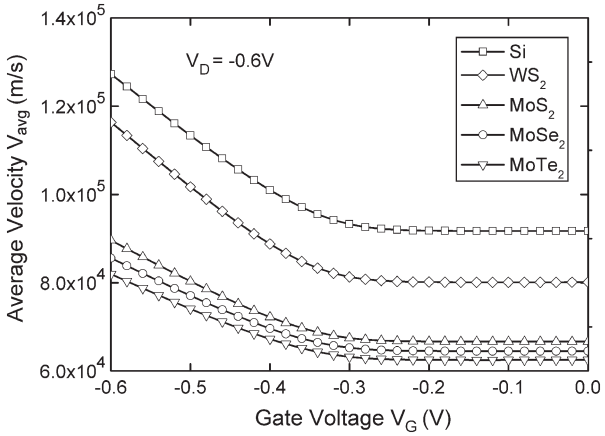

Fig. 8. Average velocity $V_{\rm avg}$ of carrier at the top of the energy barrier, with increasing gate voltage V_G for p-type monolayer MX_2 and 2-D-Si transistors. Both the heavy and light holes of Si are considered in the calculation. V_D is set at -0.6 V.

advantage of monolayer MX_2 transistors in terms of ballistic ON-current, a thin high-κ gate insulator is necessary.

For a more practical model, the influence of phonon scattering, impurity scattering, and contact resistance should be considered to provide a more complete picture, which is well beyond the simple model used in this paper.

IV. Summary

In this paper, we have first calculated the band structures of monolayer $MX_2(\mathrm{M = Mo,\ W;\ X = S,\ Se,\ Te})$, which are new 2-D semiconductors that can be effectively produced. By comparing the calculated results using different methods, we find a fixed structure with bulk lattice parameters that give results closest to the experimental data. This is because the structure of monolayer MX_2 remains the same as the bulk MX_2. Using this method, we further compute the energy band gaps and effective masses along different crystal directions. Then, we adopt a ballistic MOSFET model to evaluate the performance limits of monolayer MX_2 transistors and compare the results with those of 2-D-Si transistors. We find that the ballistic performances of monolayer MoX_2 transistors are very similar to each other, whereas monolayer WS_2 transistors have a better performance. All of them outperform 2-D-Si transistors in terms of the ballistic ON-current when a thin high-κ gate insulator is applied. Monolayer MX_2 transistors can exhibit better gate controllability because of the atomic body thickness, and thus, they are promising 2-D materials for future nanoelectronic device applications.

Note: During the review of this paper, we become aware of a paper published by A. Kuc *et al.* [31], which shows that the combination of different functional and relaxed structures, results in a similar band gap for monolayer MoS_2 transistors.

References

[1] A. K. Geim and K. S. Novoselov, "The rise of graphene," *Nat. Mater.*, vol. 6, no. 3, pp. 183–191, Mar. 2007.
[2] Y. Zhang, Y.-W. Tan, H. L. Stormer, and P. Kim, "Experimental observation of the quantum Hall effect and Berry's phase in graphene," *Nature*, vol. 438, no. 7065, pp. 201–204, Nov. 2005.
[3] X. Li, X. Wang, L. Zhang, S. Lee, and H. Dai, "Chemically derived, ultrasmooth graphene nanoribbon semiconductors," *Science*, vol. 319, no. 5867, pp. 1229–1232, Feb. 2008.
[4] L. Jiao, L. Zhang, X. Wang, G. Diankov, and H. Dai, "Narrow graphene nanoribbons from carbon nanotubes," *Nature*, vol. 458, no. 7240, pp. 877–880, Apr. 2009.
[5] F. Sols, F. Guinea, and A. H. C. Neto, "Coulomb blockade in graphene nanoribbons," *Phys. Rev. Lett.*, vol. 99, no. 16, p. 166 803, Oct. 2007.
[6] Y. Yoon and J. Guo, "Effect of edge roughness in graphene nanoribbon transistors," *Appl. Phys. Lett.*, vol. 91, no. 7, pp. 073103-1–073103-3, Aug. 2007.
[7] *Gmelin Handbook of Inorganic and Organometallic Chemistry*, 8th ed. Berlin, Germany: Springer-Verlag, 1985, p. 16.
[8] J. A. Wilson and A. D. Yoffe, "The transition metal dichalcogenides discussion and interpretation of the observed optical, electrical and structural properties," *Adv. Phys.*, vol. 18, no. 73, pp. 193–335, May 1969.
[9] R. F. Frindt, "Single crystals of MoS_2 several molecular layers thick," *J. Appl. Phys.*, vol. 37, no. 4, pp. 1928–1929, Mar. 1966.
[10] K. S. Novoselov, D. Jiang, F. Schedin, T. J. Booth, V. V. Khotkevich, S. V. Morozov, and A. K. Geim, "Two-dimensional atomic crystals," *Proc. Natl. Acad. Sci. U. S. A.*, vol. 102, no. 30, pp. 10 451–10 453, Jul. 2005.
[11] P. Joensen, R. F. Frindt, and S. R. Morrison, "Single-layer MoS_2," *Mater. Res. Bull.*, vol. 21, no. 4, pp. 457–461, Apr. 1986.
[12] J. N. Coleman, M. Lotya, A. O'Neill, S. D. Bergin, P. J. King, U. Khan, K. Young, A. Gaucher, S. De, R. J. Smith, I. V. Shvets, S. K. Arora, G. Stanton, H. Y. Kim, K. Lee, G. T. Kim, G. S. Duesberg, T. Hallam, J. J. Boland, J. J. Wang, J. F. Donegan, J. C. Grunlan, G. Moriarty, A. Shmeliov, R. J. Nicholls, J. M. Perkins, E. M. Grieveson, K. Theuwissen, D. W. McComb, P. D. Nellist, and V. Nicolosi, "Two-dimensional nanosheets produced by liquid exfoliation of layered materials," *Science*, vol. 331, no. 6017, pp. 568–571, Feb. 2011.
[13] B. Radisavljevic, A. Radenovic, J. Brivio, V. Giacometti, and A. Kis, "Single-layer MoS_2 transistors," *Nat. Nanotechnol.*, vol. 6, no. 3, pp. 147–150, Mar. 2011.

[14] G. Kresse and J. Furthmuller, "Efficient iterative schemes for *ab initio* total-energy calculations using a plane-wave basis set," *Phys. Rev. B, Condens. Matter*, vol. 54, no. 16, pp. 11 169–11 186, Oct. 1996.
[15] G. Kresse and D. Joubert, "From ultrasoft pseudopotentials to the projector augmented-wave method," *Phys. Rev. B, Condens. Matter*, vol. 59, no. 3, pp. 1758–1775, Jan. 1999.
[16] P. E. Blöchl, "Projector augmented-wave method," *Phys. Rev. B*, vol. 50, no. 24, pp. 17 953–17 979, Dec. 1994.
[17] J. P. Perdew, K. Burke, and M. Ernzerhof, "Generalized gradient approximation made simple," *Phys. Rev. Lett.*, vol. 77, no. 18, pp. 3865–3868, Oct. 1996.
[18] J. Heyd, G. E. Scuseria, and M. Ernzerhof, "Hybrid functional based on a screened Coulomb potential," *J. Chem. Phys.*, vol. 118, no. 18, pp. 8207–8215, May 2003.
[19] K. F. Mak, C. Lee, J. Hone, J. Shan, and T. F. Heinz, "Atomically thin MoS_2: A new direct-gap semiconductor," *Phys. Rev. Lett.*, vol. 105, no. 13, p. 136 805, Sep. 2010.
[20] S. Lebegue and O. Eriksson, "Electronic structure of two-dimensional crystals from *ab initio* theory," *Phys. Rev. B*, vol. 79, no. 11, p. 115 409, Mar. 2009.
[21] A. Splendiani, L. Sun, Y. Zhang, T. Li, J. Kim, C. Chim, G. Galli, and F. Wang, "Emerging photoluminescence in monolayer MoS_2," *Nano Lett.*, vol. 10, no. 4, pp. 1271–1275, Apr. 2010.
[22] T. Böker, R. Severin, A. Müller, C. Janowitz, R. Manzke, D. Vo, P. Krüger, A. Mazur, and J. Pollmann, "Band structure of MoS_2, $MoSe_2$, and $\alpha - MoTe_2$: Angle-resolved photoelectron spectroscopy and *ab initio* calculations," *Phys. Rev. B*, vol. 64, no. 23, p. 235 305, Dec. 2001.
[23] R. Manzke and M. Skibowski, *Landolt-Bornstein/New Series III 23 B: Electronic Structure of Solids: Photoemission Spectra and Related Data*, A. Goldmann, Ed. Berlin, Germany: Springer-Verlag, 1994, p. 131.
[24] W. J. Schutte, J. L. De Boer, and F. Jellinek, "Crystal structures of tungsten disulfide and diselenide," *J. Solid State Chem.*, vol. 70, no. 2, pp. 207–209, Oct. 1987.
[25] K. Natori, "Ballistic metal–oxide–semiconductor field effect transistor," *J. Appl. Phys.*, vol. 76, no. 8, pp. 4879–4890, Oct. 1994.
[26] F. Assad, Z. Ren, D. Vasileska, S. Datta, and M. S. Lundstrom, "On the performance limits for Si MOSFETs: A theoretical study," *IEEE Trans. Electron Devices*, vol. 47, no. 1, pp. 232–240, Jan. 2000.
[27] A. Rahman, J. Guo, S. Datta, and M. S. Lundstrom, "Theory of ballistic nanotransistors," *IEEE Trans. Electron Devices*, vol. 50, no. 9, pp. 1853–1864, Sep. 2003.
[28] N. Neophytou, A. Paul, M. S. Lundstrom, and G. Klimeck, "Bandstructure effects in silicon nanowire electron transport," *IEEE Trans. Electron Devices*, vol. 55, no. 6, pp. 1286–1297, Jun. 2008.
[29] G. Fiori, S. Lebegue, A. Betti, P. Michetti, M. Klintenberg, O. Eriksson, and G. Iannaccone, "Simulation of hydrogenated graphene field-effect transistors through a multiscale approach," *Phys. Rev. B*, vol. 82, no. 15, pp. 153 404-1–153 404-4, Oct. 2010.
[30] Y. Taur and T. H. Ning, *Fundamentals of Modern VLSI Devices*. New York: Cambridge Univ. Press, 1998, pp. 199–200.
[31] A. Kuc, N. Zibouche, and T. Heine, "How does quantum confinement influence the electronic structure of transition metal sulfides TmS_2," *Phys. Rev. B*, to be published.

Leitao Liu received the B.S. degree in optical engineering from Zhejiang University, Hangzhou, China, in 2010.

He is currently with the Computational Nanotechnology Laboratory, Department of Electrical and Computer Engineering, University of Florida, Gainesville, FL. His research interests include the modeling and simulation of nanoscale electron devices.

S. Bala Kumar received the Ph. D. degree in electrical engineering from the National University of Singapore, Singapore, in 2009.

He is currently a Postdoctoral Researcher with the University of Florida, Gainesville. His current research interests include the modeling and simulation of nanodevices and carbon-nanotube and graphene electronics.

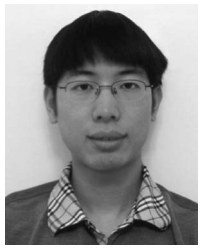

Yijian Ouyang received the B.E.E. degree from Zhejiang University, Hangzhou, China, in 2005 and the M.S. and Ph.D. degrees in electrical engineering from the University of Florida, Gainesville, in 2008 and 2011, respectively.

His research interests include the physics, modeling, and simulation of electronic devices at the nanometer scale.

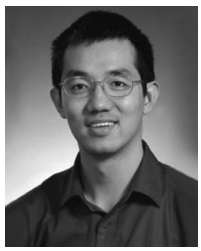

Jing Guo received the Ph. D. degree in electrical engineering from Purdue University, West Lafayette, IN, in 2004.

He is currently an Associate Professor of electrical engineering with the University of Florida, Gainesville, FL. His current research interests include the modeling and simulation of nanodevices, carbon-nanotube and graphene electronics and optoelectronics, nanowire electronics, and the device physics of nanotransistors. He is the coauthor of the book "*Nanoscale Transistors: Device Physics, Modeling, and Simulation*" (Springer-Verlag, 2006).

Dr. Guo has served in the technical program committees of International Electron Device Meeting and Device Research Conference.